2022 IEEE/ASME International Conference on
Advanced Intelligent Mechatronics (AIM)

Learning-based Safe Motion Control of Vehicle Ski-Stunt Maneuvers

Feng Han and Jingang Yi

Abstract— **This paper presents a safety guaranteed control method for an autonomous vehicle ski-stunt maneuver, i.e., a vehicle moving with two side wheels. To capture the vehicle dynamics precisely, a Gaussian process model is used as additional correction. We construct a probabilistic exponential control barrier function (CBF) to guarantee the planar motion safety. The CBF and the balance equilibrium manifold are enforced as the constraints into a safety critical control. Under the proposed control method, the vehicle can avoid the collision and safely maintain the balance for autonomous ski-stunt maneuvers. We conduct numerical simulation validation to demonstrate the control design. Preliminary experiments are also presented to confirm the learning-based motion control using a scaled truck for autonomous ski-stunt maneuvers.**

I. Introduction

Ski-stunt is a vehicle driving technique in which only two side wheels move on the ground. Vehicles in this motion can go through narrow space, pass obstacles and avoid possible collisions. Ski-stunt is one of the aggressive and agile maneuvers [1], under which the vehicle motion is unstable and may risk rolling over completely. The maneuver is usually performed by professional racing car drivers [2], [3]. There are various ways to initialize the ski-stunt maneuver and a relatively safe and tractable method is to drive the vehicle on a ramp to lift one side and then maintain the tilted body after leaving the ramp. Vehicles with high center of gravity (e.g., the sport utility vehicles and trucks) can also perform ski-stunt maneuver when turning sharply at high speed.

It is clear that the ski-stunt maneuvers is highly related to the rollover control since they share the same large roll motion and are initialized in the same way [4], [5]. Rollovers happen when vehicles turn sharply or when vehicles hit on a small obstacle at high speed [5]. Compared with the rollover, the ski-stunt motion is a balanced, safe vehicle motion. Study of the autonomous ski-stunt maneuver is of great importance for vehicle safety operation. Moreover, autonomous skit-stunt maneuvers might be used as active safety features for the next-generation of zero-accident design, particularly, in case of the emergency situation [6]–[8].

When conducting a ski-stunt maneuver, the vehicle motion is underactuated with three degrees of freedom (DOFs), that is, roll motion and planar motion, but with two control inputs (i.e., steering and velocity actuation). To prevent the vehicle from rollover or collision, safety guaranteed design must be considered. Safety critical control by the control barrier function (CBF) method is one of popular and effective approaches for autonomous robots and vehicle [9]. Safety critical control dose not explicitly design any trajectory or control inputs and instead, CBF is used as dynamic constraint to directly update the nominal control as a safety guaranteed certification in real time. Since planar motion control cannot necessarily guarantee the stable roll motion due to the underactuated property, further attention is needed to maintain the roll balance motion.

When running on two side wheels, the vehicle displays a single-track characteristic. Motion and balance control of autonomous single-track motorcycles and bicycles have been reported in the past decades [10], [11]. Steering and velocity control are among the most effective actuation for autonomous bicycles and a balance equilibrium (BEM) is used to capture the trajectory tracking and balance control simultaneously. All of the above-mentioned motion and balance control are based on physical models of vehicle dynamics [9], [12]). One challenge for autonomous ski-stunt maneuvers is the lack of accurate vehicle dynamics model. Although there are extensive research that study the rollover sequence and rollover detection [4], [5], [13], the dynamics models in those work cannot be directly used for ski-stunt maneuver control due to large roll motion.

We study and design the safety-guaranteed autonomous ski-stunt maneuver. To achieve superior performance, we build a machine learning-based model using Gaussian process (GP) to compensate for the modeling errors. A probabilistic exponential CBF is defined for planar motion safety. The control design is extended and updated through a model predictive control (MPC) method by considering the safety requirement. To prevent any possible rollover, CBFs for roll motion are also added into the design. To guarantee the balance of roll motion, the BEM is introduced to estimate the desired instantaneous equilibrium [14], [15]. Under the proposed control design, the closed-loop system is exponentially stable and the safety are guaranteed. We validate the design using a scaled trunk vehicle with simulation and experiments. The main contribution of this work lies in the new learning-based safety and balance control design for a ski-stunt maneuver. To our best knowledge, no autonomous ski-stunt maneuver was reported previously and this is the first study to demonstrate the safety-guaranteed design.

II. Learning-Enhanced Vehicle System Dynamics

A. System Configuration

Fig. 1(a) shows the scaled truck platform modified for the ski-stunt maneuvers (see Fig. 1(b)). Figs. 1(c) and 1(d) show

This work was partially supported by the US National Science Foundation under award CNS-1932370.

F. Han and J. Yi are with the Department of Mechanical and Aerospace Engineering, Rutgers University, Piscataway NJ 08854 USA (email: fh233@scarletmail.rutgers.edu, jgyi@rutgers.edu).

978-1-6654-1307-7/22/$31.00 ©2022 IEEE

(a) (b) (c) (d)

Fig. 1. (a) The scaled racing truck (modified from Traxxas X-Maxx racing truck) with Jetson TX2 computer and sensors. (b) The vehicle ski-stunt maneuver in experiment. (b) Side view and (d) back view of the schematics of the vehicle ski-stunt maneuver.

the side and back views of the vehicle. The wheelbase contact line is denoted as C_1C_2 and $l_1 = \overline{C_1C_2}$. Three coordinate frames are introduced: the initial frame $\mathcal{I}$ is fixed on the ground with upward z-axis, the body frame $\mathcal{B}$ is fixed at the truck's center of mass (CoM), and the local frame $\mathcal{H}$ is located at C_2 with x-axis along C_1C_2. We denote the position of C_2 as $\boldsymbol{r}_{C_2} = [x\, y]^T$ in $\mathcal{I}$ and it is considered as the vehicle position. The steering, yaw and roll angles are ϕ, ψ and φ, respectively. The vehicle CoM position is $\boldsymbol{r}_G = [x_G\, y_G\, z_G]^T$ in $\mathcal{H}$. The zero roll angle $\varphi = 0$ is defined as the static roll motion equilibrium point. The position of $\varphi = 0$ corresponds to that rotating the vehicle $\varphi_G = \frac{\pi}{2} - \arctan|\frac{z_G}{y_G}|$ along the x-axis in $\mathcal{H}$; see Fig. 1(d). The actual rotation angle from four-wheel driving position is $\varphi_r = \varphi + \varphi_G$. The goal is to design a control systems to allow the vehicle avoids the any obstacles while maintains the balance with running on two wheels at C_1 and C_2.

B. System Dynamics

Assuming no wheel slippage at C_1 and C_2 with the non-holonomic constraint at C_2, the vehicle velocity is given as $\dot{x} = v\cos\psi = v\,\mathrm{c}_\psi$, $\dot{y} = v\sin\psi = v\,\mathrm{s}_\psi$, where v is the velocity meganitude and notations $\mathrm{c}_\psi = \cos\psi$ and $\mathrm{s}_\psi = \sin\psi$ are used for ψ and other angles. The planar motion kinematics model is obtained as

$$\begin{bmatrix}\ddot{x}\\ \ddot{y}\end{bmatrix} = \underbrace{\begin{bmatrix}\mathrm{c}_\psi & -v\,\mathrm{s}_\psi\\ \mathrm{s}_\psi & v\,\mathrm{c}_\psi\end{bmatrix}}_{\boldsymbol{g}_r}\begin{bmatrix}\dot{v}\\ \dot{\psi}\end{bmatrix} = \boldsymbol{g}_r\boldsymbol{u}, \tag{1}$$

where $\boldsymbol{u} = [u_v\, u_\psi]$, $u_v = \dot{v}$ and $u_\psi = \dot{\psi}$ is the yaw angle rate that is related to the steering control input as [11]

$$\dot{\psi} = \frac{v}{l_1\,\mathrm{c}_{\varphi+\varphi_G}}\tan\phi. \tag{2}$$

The roll motion of the vehicle is captured by an inverted pendulum model using the Lagrangian method. The position of CoM in $\mathcal{I}$ is

$$\boldsymbol{r}_G^{\mathcal{I}} = \boldsymbol{r}' + \boldsymbol{R}_{\mathcal{H}}^{\mathcal{I}}\boldsymbol{r}_G^{\mathcal{H}} = \begin{bmatrix}r_{C_2}\\ 0\end{bmatrix} + \begin{bmatrix}x_G\,\mathrm{c}_\psi + l_G\,\mathrm{s}_\psi\,\mathrm{s}_\varphi\\ x_G\,\mathrm{s}_\psi - l_G\,\mathrm{c}_\psi\,\mathrm{s}_\varphi\\ l_G\,\mathrm{c}_\varphi\end{bmatrix}, \tag{3}$$

where $\boldsymbol{r}' = [\boldsymbol{r}_{C_2}^T\ 0]^T$, $\boldsymbol{R}_{\mathcal{H}}^{\mathcal{I}}$ transfers the vector in $\mathcal{H}$ to $\mathcal{I}$, $\boldsymbol{r}_G^{\mathcal{H}} = [x_G\ -l_G\,\mathrm{s}_\varphi\ \ l_G\,\mathrm{c}_\varphi]^T$, and $l_G = \sqrt{y_G^2 + z_G^2}$. The velocity of the CoM in $\mathcal{I}$ is obtained by taking differentiation of (3), $\boldsymbol{v}_G^{\mathcal{I}} = \dot{\boldsymbol{r}}_G^{\mathcal{I}}$. The angular velocity of the vehicle in $\mathcal{B}$ is $\boldsymbol{\omega}_G^{\mathcal{B}} = \boldsymbol{R}_{\mathcal{H}}^{\mathcal{B}}\boldsymbol{\omega}_G^{\mathcal{H}}$, $\boldsymbol{\omega}_G^{\mathcal{H}} = [\dot{\varphi}\ 0\ \dot{\psi}]^T$.

The kinetic energy of the vehicle is $T = \frac{1}{2}m(v_G^I)^2 + \frac{1}{2}(\boldsymbol{\omega}_G^{\mathcal{B}})^T\boldsymbol{J}_G\boldsymbol{\omega}_G^{\mathcal{B}}$, where $\boldsymbol{J}_G = \mathrm{diag}(J_x, J_y, J_z)$ is the moment of inertia about CoM. The potential energy is $V = mgl_G\,\mathrm{c}_\varphi$, where m is the vehicle mass. With the Lagrangian method, we obtain the roll motion dynamics

$$J_t\ddot{\varphi} - mgl_G\,\mathrm{s}_\varphi = \tau, \tag{4}$$

where $J_t = mr_G^2 + J_x$ and the steer-induced torque is $\tau = ml_Gx_G\ddot{\psi}\,\mathrm{c}_\psi + ml_G^2\dot{\psi}^2\,\mathrm{s}_\varphi\,\mathrm{c}_\varphi + \left(\mathrm{c}_\varphi^2\,J_z + \mathrm{s}_\varphi^2\,J_y\right)\dot{\psi}^2 - \left(ml_Gx_G\dot{\varphi}\,\mathrm{s}_\varphi - vl_Gm\,\mathrm{c}_\varphi\right)\dot{\psi}$. The above steer-induced torque τ captures the centrifugal force, which influences the roll motion of the vehicle [16]. Noting that $v \gg |\dot{\psi}|$ and by neglecting the second-order term and using (2), we obtain the simplified steer-induced torque as

$$\tau = mvl_G\,\mathrm{c}_\varphi\,u_\psi = \frac{mv^2l_G\,\mathrm{c}_\varphi}{l_1\,\mathrm{c}_{\varphi+\varphi_G}}\tan\phi. \tag{5}$$

Letting $f_\varphi = \frac{1}{J_t}(mgl_G\,\mathrm{s}_\varphi)$ and $g_\varphi = \frac{1}{J_t}mvl_G\,\mathrm{c}_\varphi$, the roll dynamics is written as $\ddot{\varphi} = f_\varphi + g_\varphi u_\psi$. Introducing $\boldsymbol{x} = [\boldsymbol{r}_{C_2}^T\ \varphi]^T$, the nominal model of the system is written as

$$\ddot{\boldsymbol{x}} = \begin{bmatrix}\ddot{\boldsymbol{r}}_{C_2}\\ \ddot{\varphi}\end{bmatrix} = \underbrace{\begin{bmatrix}\boldsymbol{0}\\ f_\varphi\end{bmatrix}}_{\boldsymbol{f}} + \underbrace{\begin{bmatrix}\boldsymbol{g}_r\\ g_\varphi\end{bmatrix}}_{\boldsymbol{g}}\begin{bmatrix}u_v\\ u_\psi\end{bmatrix} = \boldsymbol{f} + \boldsymbol{g}\boldsymbol{u}, \tag{6}$$

where $\boldsymbol{g}_\varphi = [0\ g_\varphi]$. It is clear that from (6) the vehicle is underactuated and the steering input affects both the planar and roll motion.

C. GP-Enhanced Model

We consider an additive term to (6) to capture unmodeled dynamics and uncertainties, i.e.,

$$\ddot{\boldsymbol{x}} = \boldsymbol{f} + \boldsymbol{g}\boldsymbol{u} + \boldsymbol{f}_u, \tag{7}$$

where $\boldsymbol{f}_u = [f_{ux}\ f_{ux}\ f_{u\varphi}]^T$ denotes the unmodeled effects and uncertainties that are invariant under varying position $\boldsymbol{r}_{C_2}$. A GP model is used to estimate $\boldsymbol{f}_u$ that is related to state $\boldsymbol{\xi} = [\dot{x}\ \dot{y}\ \ddot{x}\ \ddot{y}\ \varphi\ \dot{\varphi}\ \ddot{\varphi}\ \phi\ v\,]^T \in \mathbb{R}^9$. $\boldsymbol{f}_w = \boldsymbol{f}_u(\boldsymbol{\xi}) + \boldsymbol{w}$ is denoted as the noisy observation of $\boldsymbol{f}_u$, where $\boldsymbol{w} \sim \mathcal{N}(\boldsymbol{0}, \boldsymbol{\Sigma})$ is the zero-mean Gaussian noise. We use the GP regression to capture $\boldsymbol{f}_u$. The training data set is $\boldsymbol{D} = \{\boldsymbol{X}, \boldsymbol{Y}\} = \{\{\boldsymbol{\xi}_i\}_{i=1}^N, \{\boldsymbol{f}_{wi}\}_{i=1}^N\}$, where N is the number of training data points and $\boldsymbol{f}_w$ is

obtained as the difference between actual measurement and nominal model calculation.

The GP for f_{ux}, for instance, is to maximize the likelihood functionlog$(\boldsymbol{Y}_x; \boldsymbol{X}, \boldsymbol{\theta}) = -\frac{1}{2}\boldsymbol{Y}_x^T\boldsymbol{K}^{-1}\boldsymbol{Y}_x - \frac{1}{2}\log\det(\boldsymbol{K})$, where $K_{ij} = k(\boldsymbol{\xi}_i, \boldsymbol{\xi}_j) = \sigma_f^2 \exp(-\frac{1}{2}(\boldsymbol{\xi}_i - \boldsymbol{\xi}_j)^T\boldsymbol{W}(\boldsymbol{\xi}_i - \boldsymbol{\xi}_j)) + \sigma_0^2\delta_{ij}$, $\boldsymbol{W} = \text{diag}\{W_1, \cdots, W_m\}$, $\delta_{ij} = 1$ for $i = j$ only, $\boldsymbol{\theta} = \{\boldsymbol{W}, \sigma_f, \sigma_0\}$, and $\boldsymbol{Y}_x$ is the vector composed by all f_{wx} in $\boldsymbol{D}$. Given the new measurement data $\boldsymbol{\xi}^*$, GP regression predicts the mean value and the standard deviation of the unmodeled dynamics as

$$\mu(\boldsymbol{\xi}^*) = \boldsymbol{k}^T\boldsymbol{K}^{-1}\boldsymbol{Y}_x,\ \Sigma(\boldsymbol{\xi}^*) = k^* - \boldsymbol{k}^T\boldsymbol{K}^{-1}\boldsymbol{k}, \tag{8}$$

where $\boldsymbol{k} = \boldsymbol{k}(\boldsymbol{\xi}^*, \boldsymbol{X})$ and $k^* = k(\boldsymbol{\xi}^*, \boldsymbol{\xi}^*)$. The predictions for f_y and f_φ are obtained in the same manner. We then use the prediction $\boldsymbol{f}_\mu(\boldsymbol{\xi}) = [f_{\mu x}(\boldsymbol{\xi})\ f_{\mu y}(\boldsymbol{\xi})\ f_{\mu\varphi}(\boldsymbol{\xi})]^T$ to approximate $\boldsymbol{f}_u$. Furthermore, the prediction error $\boldsymbol{\delta}_f = \boldsymbol{f}_u(\boldsymbol{\xi}) - \boldsymbol{f}_\mu(\boldsymbol{\xi})$ is bounded in the sense of probability as shown in the following Lemma.

Lemma 1 ([17]): Given $\boldsymbol{D}$, if the kernel function $k(\boldsymbol{\xi}_i, \boldsymbol{\xi}_j)$ is chosen such that f_{ui} has a finite reproducing kernel Hilbert space norm $\|\boldsymbol{f}_u\|_{\boldsymbol{k}} < \infty$, for given $0 < \eta < 1$,

$$\Pr\left\{\|\boldsymbol{\delta}_f\| \le \|\boldsymbol{\Sigma}^{\frac{1}{2}}(\boldsymbol{\xi})\boldsymbol{\kappa}\|\right\} \ge \eta, \tag{9}$$

where $\Pr(\cdot)$ denotes the probability of an event, $\eta \in (0, 1)$, $\boldsymbol{\kappa}, \boldsymbol{\varsigma} \in \mathbb{R}^m$, $\kappa_i = \sqrt{2|f_{ui}|_{\boldsymbol{k}}^2 + 300\varsigma_i \ln^3 \frac{N}{1-\eta^{\frac{1}{m}}}}$, $\varsigma_i = \max_{\boldsymbol{\xi}, \boldsymbol{\xi}' \in \boldsymbol{X}} \frac{1}{2}\ln|1 + \sigma_i^{-2}k_i(\boldsymbol{\xi}, \boldsymbol{\xi}')|$, and $i = 1, 2, 3$ for the dimensional elements of $\boldsymbol{f}_u$.

Defining $\boldsymbol{\chi} = [\boldsymbol{x}^T\ \dot{\boldsymbol{x}}^T]^T$, the GP-enhanced dynamics model is obtained from (7) as

$$\dot{\boldsymbol{\chi}} = \underbrace{\begin{bmatrix}\dot{\boldsymbol{x}}\\ \boldsymbol{f}\end{bmatrix}}_{\boldsymbol{F}} + \underbrace{\begin{bmatrix}\boldsymbol{0}\\ \boldsymbol{f}_u\end{bmatrix}}_{\boldsymbol{F}_\mu} + \underbrace{\begin{bmatrix}\boldsymbol{0}\\ \boldsymbol{g}\end{bmatrix}}_{\boldsymbol{G}}\boldsymbol{u} + \underbrace{\begin{bmatrix}\boldsymbol{0}\\ \boldsymbol{\delta}_f\end{bmatrix}}_{\boldsymbol{\delta}_F} = \boldsymbol{F} + \boldsymbol{F}_\mu + \boldsymbol{G}\boldsymbol{u} + \boldsymbol{\delta}_F,$$

where $\boldsymbol{F}_\mu$, $\boldsymbol{F}$, $\boldsymbol{G}$ and $\boldsymbol{\delta}_F$ are in proper dimensions.

III. Safe Ski-Stunt Maneuver Control

A. Control Barrier Function with Learning Model

For ski-stunt motion, we design learning-based CBF control strategy to prevent possible collisions and rollover. The interpretation of the safety is that the state of the vehicle dynamics systems remains in a set defined by $\mathcal{S} = \{\boldsymbol{\chi} : h(\boldsymbol{\chi}) \ge 0\}$, where $h(\cdot)$ is a continuously differential function. Set $\mathcal{S}$ is referred as a safe set of the vehicle motion. We assume that $h(\boldsymbol{\chi})$ has the relative degree $p \in \mathbb{N}$, that is, the control input $\boldsymbol{u}$ appears in the pth derivative of $h(\boldsymbol{\chi})$ explicitly. To consider the general case of the safety requirement, the explicit form of $h(\boldsymbol{\chi})$ is not specified here.

To define the CBF for the nonparametric model (7), we introduce variable $\boldsymbol{q}(\boldsymbol{\chi}) \in \mathbb{R}^p$ as

$$\boldsymbol{q}(\boldsymbol{\chi}) = [h(\boldsymbol{\chi}) \cdots h^{(p-1)}(\boldsymbol{\chi})]^T = [h(\boldsymbol{\chi}) \cdots L_F^{p-1}h(\boldsymbol{\chi})]^T$$

and Lie derivative $L_F h(\boldsymbol{\chi}) = L_F h(\boldsymbol{\chi}) + L_{F\mu}h(\boldsymbol{\chi})$. The dynamics of $\boldsymbol{q}(\boldsymbol{\chi})$ is obtained as

$$\dot{\boldsymbol{q}} = \boldsymbol{A}\boldsymbol{q} + \boldsymbol{B}\boldsymbol{u}_h + \boldsymbol{u}_\delta,\ h = \boldsymbol{C}\boldsymbol{q} \tag{10}$$

with

$$\boldsymbol{A} = \begin{bmatrix}0 & \boldsymbol{I}_{p-1}\\ 0 & \boldsymbol{0}\end{bmatrix}, \boldsymbol{B} = \begin{bmatrix}\boldsymbol{0}\\ 1\end{bmatrix}, \boldsymbol{C} = \begin{bmatrix}1 & \boldsymbol{0}\end{bmatrix}, \boldsymbol{u}_\delta = \begin{bmatrix}\boldsymbol{0}\\ \frac{\partial h}{\partial \boldsymbol{\chi}}\boldsymbol{\delta}_F\end{bmatrix},$$

where $\boldsymbol{I}_{p-1}$ represents the identity matrix of dimension $p-1$, $u_h = L_F^p h(\boldsymbol{\chi}) + L_G L_F^{p-1}h(\boldsymbol{\chi})\boldsymbol{u}$, and $L_G L_F^{p-1}h(\boldsymbol{\chi})$ is assumed to be invertible.

A feedback gain $\boldsymbol{\gamma}$ is selected properly such that the unperturbed system $(\boldsymbol{A}, \boldsymbol{B}, \boldsymbol{C})$ with $\boldsymbol{u}_\delta = \boldsymbol{0}$ with control input $\boldsymbol{u}_h = -\boldsymbol{\gamma}\boldsymbol{q}$ is exponentially stable. The solution of $h(\boldsymbol{\chi})$ is

$$\begin{aligned} h(\boldsymbol{\chi}) &= \underbrace{\boldsymbol{C}e^{-(\boldsymbol{A}-\boldsymbol{B}\boldsymbol{\gamma})t}\boldsymbol{q}(0)}_{h_u(\boldsymbol{\chi})} + \underbrace{\int_0^t \boldsymbol{C}e^{(\boldsymbol{A}-\boldsymbol{B}\boldsymbol{\gamma})\nu}\boldsymbol{u}_\delta(t-\nu)d\nu}_{h_\delta(\boldsymbol{\chi})},\\ &= h_u(\boldsymbol{\chi}) + h_\delta(\boldsymbol{\chi}), \end{aligned}$$

If the model is exactly accurate, namely, $h_\delta(\boldsymbol{\chi}) = 0$, $h(\boldsymbol{\chi})$ is referred as the exponential CBF, when $\boldsymbol{u}_h > -\boldsymbol{\gamma}\boldsymbol{q}$ and $h_u(\boldsymbol{\chi}) \ge \boldsymbol{C}e^{(\boldsymbol{A}-\boldsymbol{B}\boldsymbol{\gamma})t}\boldsymbol{q}(0) > 0$, for $t > 0$ and $h_u(0) > 0$ [18], [19]. Assuming that $h(\boldsymbol{\chi})$ is locally Lipschitz in $\boldsymbol{\chi} \in \mathcal{S}$, namely, $\|\frac{\partial h}{\partial \boldsymbol{\chi}}\| \le M_h$ with finite number $M_h > 0$, $\boldsymbol{u}_\delta$ can be shown as probabilistically bounded $\Pr\left\{\|\boldsymbol{u}_\delta\| \le M_h\|\boldsymbol{\Sigma}^{\frac{1}{2}}(\boldsymbol{\xi})\boldsymbol{\kappa}\|\right\} \ge \eta$. Then $h_\delta(\boldsymbol{\chi})$ is bounded with probability $\Pr\{|h_\delta| \le h_\delta^{\max}\} \ge \eta$, where $h_\delta^{\max} = \sup_{\{\boldsymbol{\delta}_F, t\}}\int_0^t \boldsymbol{C}e^{(\boldsymbol{A}-\boldsymbol{B}\boldsymbol{\gamma})\nu}\boldsymbol{u}_\delta(t-\nu)d\nu$ for all possible GP prediction errors and experiment time.

Definition 1: Probabilistic exponential control barrier function: Given the nonparametric dynamics (7), the function $h(\boldsymbol{\chi})$ is a *probabilistic exponential CBF* if there exists $\boldsymbol{\gamma}$ such that

$$\sup_{\boldsymbol{u}\in\mathcal{U}}\left[L_F^p h(\boldsymbol{\chi}) + L_G L_F^{p-1}h(\boldsymbol{\chi})\boldsymbol{u}\right] \ge -\boldsymbol{\gamma}\boldsymbol{q}(\boldsymbol{\chi}), \tag{11}$$

where $\mathcal{U}$ is the feasible control set and $h(\boldsymbol{\chi}) = h_1(\boldsymbol{\chi}) - h_2(\boldsymbol{\Sigma}(\boldsymbol{\xi}))$ with $h_1(\boldsymbol{\chi})$ denoting the nominal function, $h_2(\boldsymbol{\Sigma}(\boldsymbol{\xi}))$ being introduced to account for the GP prediction uncertainties. $h_2(\boldsymbol{\Sigma}(\boldsymbol{\xi}))$ is chosen as $h_2(\boldsymbol{\Sigma}(\boldsymbol{\xi})) = \boldsymbol{\Sigma}(\boldsymbol{\xi})$ [20]. Meanwhile, if $\boldsymbol{u}$ satisfies (11), function $h(\boldsymbol{\chi})$ has

$$\Pr\{h(\boldsymbol{\chi}) \ge -h_\delta^{\max}\} \ge \eta. \tag{12}$$

Compared with the conventional CBF, $h(\boldsymbol{\chi})$ might reach to a negative value. However, with sufficient training data, GP prediction error could be small [17] and therefore, $h_\delta^{\max} \ll 1$. In practice, a safety buffer zone can be added when designing the nominal CBF by considering the vehicle size, which is interpreted as to define the safety criterion conservatively. Furthermore, the CBF in (12) incorporates the probability property of GP regression, which is not involved in other work [20].

B. Ski-Stunt Maneuver Control

With the CBF designed above, the ski-stunt maneuver control is formulated in a safety critical control form [18]. The set of safety guaranteed control is defined as

$$\mathcal{U}_s = \{\boldsymbol{u} \in \mathcal{U} : L_F^p h(\boldsymbol{\chi}) + L_G L_F^{p-1}h(\boldsymbol{\chi})\boldsymbol{u} \ge -\boldsymbol{\gamma}\boldsymbol{q}(\boldsymbol{\chi})\}.$$

Given the nominal control $\boldsymbol{u}$, we solve the safe control by minimizing $\boldsymbol{e}_u^T \boldsymbol{e}_u$ under constraints $\boldsymbol{u}_s \in \mathcal{U}_s$, $\boldsymbol{e}_u = \boldsymbol{u}_s - \boldsymbol{u}$, and $\boldsymbol{u}_s$ is the target safe control.

The safety criteria is the collision avoidance with multiple obstacles for the planar motion and rollover prevention for the roll motion, especially in the initialization phase. We design CBF $h(\boldsymbol{\chi}) = h(\varphi)$ in terms of the roll motion to safely move roll angle to desired profile and prevent a complete rollover. We take above planar motion safety and rollover prevention into the control design. To further strengthen the safety, we formulate the planar motion safe control design as a MPC problem as

$$\min_{\boldsymbol{u}_H} \int_t^{t+t_H} \boldsymbol{e}^T \boldsymbol{W}_1 \boldsymbol{e} + \boldsymbol{e}_u^T \boldsymbol{W}_2 \boldsymbol{e}_u dt, \tag{13a}$$

$$\text{subj. to}: \ddot{\boldsymbol{x}}(\varsigma) = \boldsymbol{f}_\mu + \boldsymbol{f} + \boldsymbol{g}\boldsymbol{u}_s, \varsigma \in [t, t+t_H] \tag{13b}$$

$$L_F^p h_i(\boldsymbol{r}) + L_G L_F^{p-1} h_i(\boldsymbol{r}) \boldsymbol{u}_s \geq -\gamma_i \boldsymbol{q}_i(\boldsymbol{r}), \tag{13c}$$

$$L_F^p h_j(\varphi) + L_G L_F^{p-1} h_j(\varphi) \boldsymbol{u}_s \geq -\gamma_j \boldsymbol{q}_j(\varphi), \tag{13d}$$

where $\boldsymbol{u}_H = \{\boldsymbol{u}_{s1}, \cdots, \boldsymbol{u}_{sH}\}$ is the H-step control input set, $t_H = H\Delta t$ is the H-step prediction horizon, Δt is the step length, and $H \in \mathbb{N}$ is the predictive horizon. $\boldsymbol{e} = \boldsymbol{\chi}_d - \boldsymbol{\chi}$, $\boldsymbol{\chi}_d$ is the desired state, $\boldsymbol{e}_u = \boldsymbol{u}_s - \boldsymbol{u}$, and $\boldsymbol{W}_1 \in \mathbb{R}^6, \boldsymbol{W}_2 \in \mathbb{R}^2$ are positive definite diagonal matrices, $h_i(\boldsymbol{r})$ ($h_j(\varphi)$) is the ith (jth) CBF for planar motion (rollover prevention), $i = 1, \cdots, n_i$, $j = 1, \cdots, n_j$, $n_i, n_j \in \mathbb{N}$ are the numbers of CBFs for planar motion and rollover prevention, respectively. $h_i(\boldsymbol{r})$ and $h_j(\varphi)$ are defined in the same way as $h(\boldsymbol{\chi})$ with other elements being zeros. The optimization problem is solved online in real time via gradient descending algorithm (e.g., sequential quadratic programming).

To guarantee the balance of roll motion, we first compute the BEM and regulate the roll motion around the BEM. The BEM is defined as set of instantaneous equilibrium angles, i.e., $\mathcal{E} = \{\varphi^e : f_\varphi(\varphi^e) + f_{\mu\varphi}(\varphi^e) + g_\varphi(\varphi^e) u_{sv} = 0\}$, where u_{sv} is the planar motion controller [10]. We estimate the BEM by minimizing the following function

$$\min_\varphi \Gamma = (f_\varphi(\varphi) + f_{\mu\varphi}(\varphi) + g_\varphi(\varphi) u_{sv})^2,$$

which is solved numerically: $\varphi_{i+1}^e = \varphi_i^e - \alpha \frac{\partial \Gamma}{\partial \varphi}\Big|_{\varphi_i^e}$, $\frac{\partial \Gamma}{\partial \varphi} = 2\Gamma \left(\frac{\partial f_\varphi}{\partial \varphi} + \frac{\partial g_\varphi}{\partial \varphi} u_{s\psi} + \frac{\partial f_{\mu\varphi}}{\partial \varphi} \right)$, $\frac{\partial f_{\mu\varphi}}{\partial \varphi} = \boldsymbol{Y}_\varphi^T \boldsymbol{K}^{-1} \frac{\partial \boldsymbol{k}}{\partial \boldsymbol{\xi}} \frac{\partial \boldsymbol{\xi}}{\partial \varphi}$ with $\boldsymbol{k}$ is given by the GP model estimate (8), $\alpha > 0$ and the iteration is terminated when $\Gamma(\varphi_i^e) \leq \epsilon$ for $\epsilon > 0$. The control input is finally updated by incorporating the BEM as

$$u_{\varphi\psi} = g_\varphi^{-1}(-f_\varphi - f_{\mu\varphi} + \ddot{\varphi}^e - k_p e_\varphi - k_d \dot{e}_\varphi) \tag{14}$$

to enforce the roll motion moving around $\mathcal{E}$, where $e_\varphi = \varphi - \varphi^e$ and $k_p, k_d > 0$ are feedback gains. The final control is $\boldsymbol{u}_s^f = [u_{sv}\ u_{\varphi\psi}]$. In the simulation and experiment, we use the CBF designed control to prorogate the system state as the reference trajectory and then design the control input. By doing this, we are trying to avoid any unreasonable control design by (13). The stability of the system is summarized in the following based on the Theorem 1 in [14].

Lemma 2: Assuming that BEM estimation error (i.e., the GP regression error δ_f and the numerical BEM estimation error is locally Lipschitz and affine with the planar and roll motion errors $\boldsymbol{e}$. The system under the control $\boldsymbol{u}_s^f$ is stable with high probability and the error of the closed system converges into a small ball around zero exponentially, that is, $\boldsymbol{\chi} \in \mathcal{S}$ and $\varphi \in \mathcal{E}$.

IV. Simulation and Experimental Results

A. Experimental Setup

The scaled racing truck was built on an RC platform (model X-Maxx) from Traxxas. We installed the encoders and the inertia measurement unit (IMU) for onboard measurement. A Jetson TX2 computer and a Teensy 4.0 microcontroller were used for onboard computation purpose. The physical model parameters are $m = 11.4$ kg, $J_t = 1.35$ kgm^2, $l_1 = 0.48$ m, $y_G = 0.25$ m, $z_G = 0.29$ m $\varphi_G = 40$ deg.

In the simulation, the unmodeled dynamics were considered as $f_{ux} = 0.5v\cos^2\psi\sin\psi$, $f_{uy} = 0.5v\cos\psi\sin\psi$, $f_{u\varphi} = 0.25v^2\sin\varphi - 0.25\dot{\varphi}$ and we set $J_t = 1$ kgm^2. The training data were generated using the nominal model with arbitrarily designed input. The obstacles had a circular shape with radius R. The vehicle should avoid the obstacles while keeping balance. Furthermore, from autonomous four-wheel driving to ski-stunt maneuvers, any possible rollovers should also be avoided. Based on those requirement, the CBFs used were

$$\begin{aligned} h_i(\boldsymbol{r}) &= (R + R_\epsilon)^2 - (x - x_{ci})^2 - (y - y_{ci})^2 - \Sigma_x - \Sigma_y, \\ h(\varphi) &= (\varphi_{\max} + \varphi_G)^2 - (\varphi + \varphi_G)^2 - \Sigma_\varphi, \\ h(\dot{\varphi}) &= \dot{\varphi}_{\max}^2 - \dot{\varphi}^2, \end{aligned}$$

where (x_{ci}, y_{ci}) is the center position of the ith obstacle, R_ϵ is used to account for the GP regression error (h_δ) and serves as a buffer zone. $\varphi_{\max}$ is allowed maximum roll angle and $\dot{\varphi}_{\max}$ denotes the maximum roll angular velocity.

In simulation and experiment, the truck's velocity was set at a constant value, which left the steering as the only control actuation for planar motion and roll motion. The control parameters used in design were $\gamma_i = [1\ 1.5]^T$, $k_p = 35$, $k_d = 20$, $\boldsymbol{W}_1 = \text{diag}\{20, 20, 20, 10, 10, 10\}$, $\boldsymbol{W}_2 = \text{diag}\{5, 5\}$, $\alpha = 0.05$, $\epsilon = 0.005$, and $\Delta t = 0.02$ s. The computer platform used for simulation was equipped with a Core i7-9700 @ 3.0G Hz $\times$ 8 CPU.

B. Simulation Result

We first show the results with different MPC prediction horizons. The simulation was setup with an obstacle ($R = 2.5$ m and $R_\epsilon = 0.5$ m) at $(5, 5)$ m. The vehicle needs to move to the target location $(10, 10)$ m safely. Fig. 2 shows the trajectory, the roll angles, the steering angles and the CBF profiles. In all cases, the truck passed obstacle (Fig. 2(d)) with the CBF applied while closely contacting the buffer zone. Without the buffer zone, the vehicle closely passed by the obstacle. For all successful obstacle avoidance cases, the vehicle trajectories in Fig. 2(a) look similar. The differences in roll angle profile are significant as shown in Fig. 2(b). With

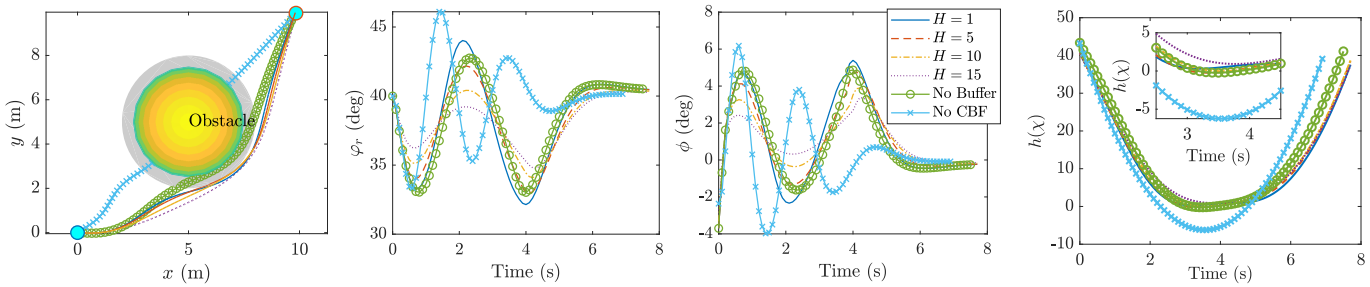

(a) (b) (c) (d)

Fig. 2. Simulation results of truck ski-stunt maneuver with different prediction horizons. (a) Truck trajectory. The gray area denotes the buffer zone and the two circle markers show the start and target locations. (b) Roll angle. (c) Steering angle. (d) CBF value.

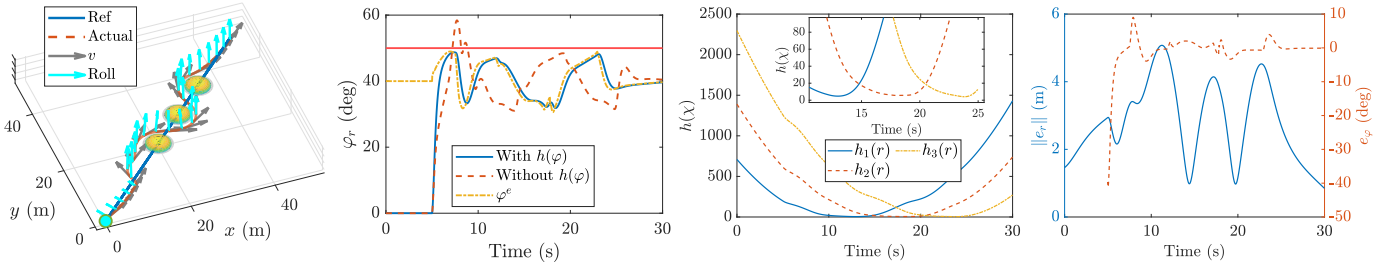

(a) (b) (c) (d)

Fig. 3. Simulation results of a straight line tracking task with multiple obstacles. (a) Truck trajectory. (b) Roll angle. The horizontal line in denotes $\varphi_{\max} = 10$ deg ($\varphi_{\max} + \varphi_G = 50$ deg). (c) CBF value. (d) Position and roll angle tracking errors.

increased prediction horizons, the roll angle changes become small. Since the desired roll angle was calculated through the BEM, a large roll angle indicates that the curvature of the trajectory is large and therefore it is difficult to follow (large steering angle change is needed; see Fig. 2(c)). For the tradeoff between computation cost and trajectory tracking performance, we chose $H = 5$ in the following tests.

We demonstrate a tracking task with multiple obstacles. The reference trajectory is $x_d = y_d = 1.6t$. Three obstacles were at $(20, 20)$, $(27.5, 27.5)$, and $(35, 35)$ m. For safety concern, the maximum roll angle was set at 10 deg. Thus the CBFs considered were $h_1(\boldsymbol{r}), h_2(\boldsymbol{r}), h_3(\boldsymbol{r})$ and $h(\varphi)$. Fig. 3(a) shows a 3-D illustration with the velocity direction and roll angle direction added to the trajectory. In the first 5 s, the truck was in the four-wheel driving mode. At $t = 5$ s, the truck conducted a sharp turn to initialize the ski-stunt maneuver. Compared with the case without roll motion CBF, the roll angle was less than 10 deg; see Fig. 3(b). The truck successfully passed three obstacles in an "S"-shape trajectory as shown in Fig. 3(c). The arrows marked "Roll" in Fig. 3(a) indicate the roll angle changes to maintain balance. Fig. 3(b) shows the reference roll angle (i.e., BEM) and the roll angle closely followed the reference. Fig. 3(d) shows the planar and roll motion errors and both of them decay to zero.

C. Experimental Result

Fig. 1(b) shows an experimental setup. To protect the vehicle from any possible damages by rollover, a training wheel was added and mounted on one side. When the training wheel touches down on the ground, $\varphi = 5$ deg (equivalently 45 deg rotation from four-wheel driving situation, that is, $\varphi_G = 45$ deg). Fig. 4 shows the straight line tracking experiment result based on the nominal model. For different velocities the trajectory errors were less that 0.6 m in Fig. 4(a) and the roll angle vibrate around the equilibrium point. One advantage with large velocity is that the steering induced balance torque is significant; see (5). For $t = 3$ to 4 s, the roll angles for three trials were at 38 degs and the steering angle under the small velocity $v = 0.8$ m/s is indeed the largest among $v = 0.8$, 1.2 and 1.6 m/s, as shown in Figs. 4(b) and 4(c).

Fig. 5 shows the obstacle avoidance experimental result. The analytical model was used and the MPC prediction horizon is set as $H = 5$. The obstacle center position is $(x_c, y_c) = (4, 0)$, $R = 0.8$ m, $v = 1.2$ m/s. With the CBF constraint applied, the truck passed by the obstacle and maintained the balance, although the truck is very close to the obstacle (see Fig. 5(c)). However, the truck was not able to track the reference trajectory afterwards and displays large errors. One possible reason is that the roll motion model is not accurate, which causes tracking errors in both planar motion and roll motion. The preliminary results validate the analytical model and the control design.

V. Conclusion

This paper presented the control system design for autonomous ski-stunt maneuvers. We considered the collision of planar motion and balance of the roll motion as the vehicle became underactuated and inherently unstable during the ski-stunt maneuver. To achieve superior performance, the system model was enhanced by a Gaussian process regression method.

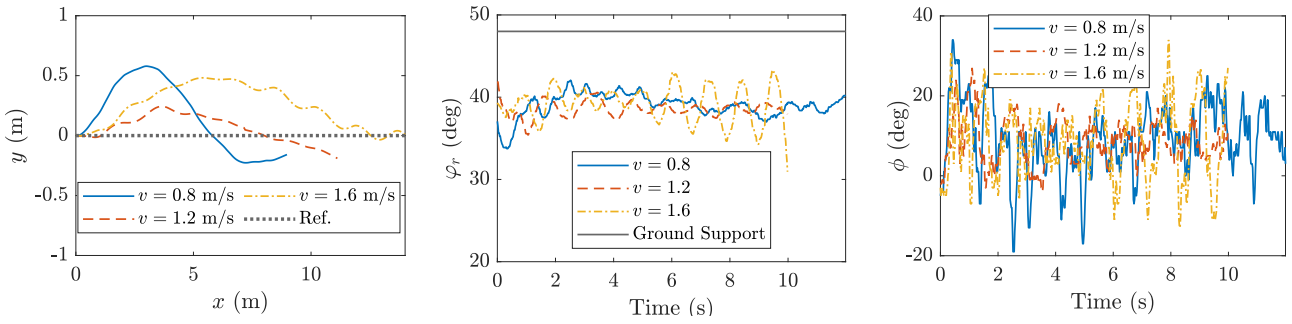

(a) (b) (c)

Fig. 4. Straight line tracking at different velocities $v = 0.8, 1.2, 1.6$ m/s. (a) Vehicle trajectories. (b) Vehicle roll angles. (c) Steering angles.

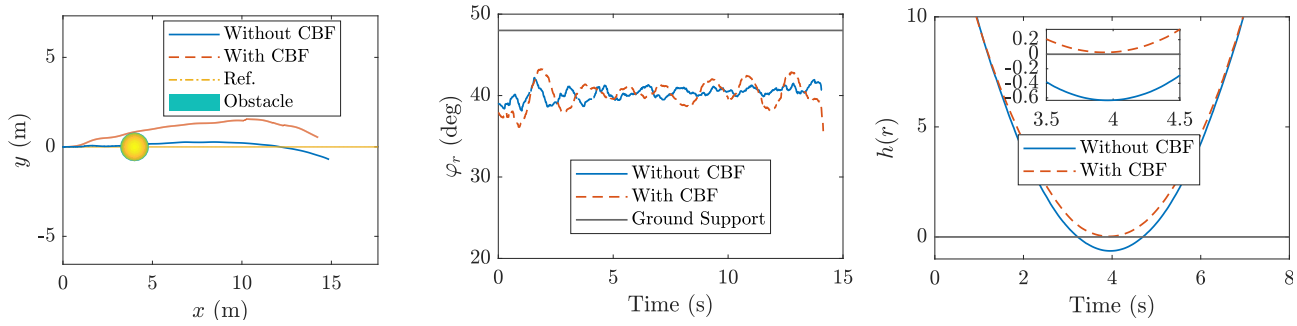

(a) (b) (c)

Fig. 5. Obstacle avoidance in ski-stunt maneuvering. (a) Vehicle trajectory. (b) Vehicle roll angles. (c) CBF function values.

We designed a model predictive control that incorporated a probabilistic exponential control barrier function method for collision avoidance and roll motion balance. Under the proposed control design, the ski-stunt maneuver was proved to be stable and safe. The control algorithm was validated through multiple numerical simulation examples and preliminary experiment. We are currently working to extend the experiments to demonstrate the performance under the proposed modeling and control design.

VI. Acknowledgment

The authors would like to thank Drs. Ali Arab and Kuo Chen for their constructive discussions and suggestions for autonomous ski-stunt maneuvers.

References

[1] J. Yi, J. Li, J. Lu, and Z. Liu, "On the dynamic stability and agility of aggressive vehicle maneuvers: A pendulum-turn maneuver example," *IEEE Trans. Contr. Syst. Technol.*, vol. 20, no. 3, pp. 663–676, 2012.

[2] B. Howell, *Monster Trucks: Tearing It Up*. Minneapolis, MN: Lerner Publications, 2014.

[3] Moderator. (2017) Chrysler at the 1964 world's fair: Hell drivers and more. [Online]. Available: https://www.allpar.com/threads/chrysler-at-the-1964-world%E2%80%99s-fair-hell-drivers-and-more.227848/

[4] R. Eger and U. Kiencke, "Modeling of rollover sequences," *IFAC Proc.*, vol. 33, no. 26, pp. 121–126, 2000.

[5] G. Phanomchoeng and R. Rajamani, "New rollover index for the detection of tripped and untripped rollovers," *IEEE Trans. Ind. Electron.*, vol. 60, no. 10, pp. 4726–4736, 2013.

[6] B. Springfeldt, "Rollover of tractors — international experiences," *Safety Science*, vol. 24, no. 2, pp. 95–110, 1996.

[7] M. Matolcsy, "The severity of bus rollover accidents," *Scientific Society of Mechanical Engineers*, pp. 1–10, 2007, paper number 989.

[8] H. Imine, L. M. Fridman, and T. Madani, "Steering control for rollover avoidance of heavy vehicles," *IEEE Trans. Veh. Technol.*, vol. 61, no. 8, pp. 3499–3509, 2012.

[9] A. Arab, I. Hadžić, and J. Yi, "Safe predictive control of four-wheel mobile robot with independent steering and drive," in *Proc. Amer. Control Conf.*, 2021, pp. 2962–2967.

[10] F. Han, A. Jelvani, J. Yi, and T. Liu, "Coordinated pose control of mobile manipulation with an unstable bikebot platform," *IEEE/ASME Trans. Mechatronics*, 2022, in press.

[11] P. Wang, J. Yi, and T. Liu, "Stability and control of a rider-bicycle system: Analysis and experiments," *IEEE Trans. Automat. Sci. Eng.*, vol. 17, no. 1, pp. 348–360, 2020.

[12] D. Bianchi, A. Borri, B. Castillo–Toledo, M. D. Benedetto, and S. D. Gennaro, "Active control of vehicle attitude with roll dynamics," *IFAC Proc.*, vol. 44, no. 1, pp. 7174–7179, 2011.

[13] J. Lu, D. Messih, and A. Salib, "Roll rate based stability control - The roll stability control system," in *Proc. 20th Int. Tech. Conf. Enhanced Safety of Veh.*, Lyon, France, June 2007, article # 07-0136.

[14] F. Han and J. Yi, "Stable learning-based tracking control of underactuated balance robots," *IEEE Robot. Automat. Lett.*, vol. 6, no. 2, pp. 1543–1550, 2021.

[15] N. Getz, "Dynamic inversion of nonlinear maps with applications to nonlinear control and robotics," Ph.D. dissertation, Dept. Electr. Eng. and Comp. Sci., Univ. Calif., Berkeley, CA, 1995.

[16] Y. Tanaka and T. Murakami, "A study on straight-line tracking and posture control in electric bicycle," *IEEE Trans. Ind. Electron.*, vol. 56, no. 1, pp. 159–168, 2009.

[17] T. Beckers, D. Kulić, and S. Hirche, "Stable gaussian process based tracking control of euler–lagrange systems," *Automatica*, vol. 103, pp. 390–397, 2019.

[18] A. D. Ames, S. Coogan, M. Egerstedt, G. Notomista, K. Sreenath, and P. Tabuada, "Control barrier functions: Theory and applications," in *Proc. Europ. Control Conf.*, Naples, Italy, 2019, pp. 3420–3431.

[19] Q. Nguyen and K. Sreenath, "Exponential control barrier functions for enforcing high relative-degree safety-critical constraints," in *Proc. Amer. Control Conf.*, Boston, MA, 2016, pp. 322–328.

[20] M. Khan, T. Ibuki, and A. Chatterjee, "Safety uncertainty in control barrier functions using gaussian processes," in *Proc. IEEE Int. Conf. Robot. Autom.*, Xian, China, 2021, pp. 6003–6009, virtual.